Transition-Metal Catalysis

How to cite: *Angew. Chem. Int. Ed.* **2022**, *61*, e202207536
International Edition: doi.org/10.1002/anie.202207536
German Edition: doi.org/10.1002/ange.202207536

Nickel-Catalyzed Enantioselective Reductive Alkyl-Carbamoylation of Internal Alkenes

Xianqing Wu[+], Aneta Turlik[+], Baixue Luan, Feng He, Jingping Qu, K. N. Houk, and Yifeng Chen**

Abstract: Herein, we leverage the Ni-catalyzed enantioselective reductive dicarbofunctionalization of internal alkenes with alkyl iodides to enable the synthesis of chiral pyrrolidinones bearing vicinal stereogenic centers. The application of newly developed $^{1\text{-Nap}}$Quinim is critical for formation of two contiguous stereocenters in high yield, enantioselectivity, and diastereoselectivity. This catalytic system also improves both the yield and enantioselectivity in the synthesis of α,α-dialkylated γ-lactams. Computational studies reveal that the enantiodetermining step proceeds with a carbamoyl-Ni^{I} intermediate that is reduced by the Mn reductant prior to intramolecular migratory insertion. The presence of the *t*-butyl group of the Quinim ligand leads to an unfavorable distortion of the substrate in the TS that leads to the minor enantiomer. Calculations also support an improvement in enantioselectivity with $^{1\text{-Nap}}$Quinim compared to $^{p\text{-tol}}$Quinim.

Introduction

Transition metal-catalyzed dicarbofunctionalization of alkenes has emerged as a versatile synthetic tool for the rapid construction of complex and useful molecules from simple chemical feedstocks.[1,2] In particular, Ni-catalyzed enantioselective reductive dicarbofunctionalization of alkenes is currently undergoing rapid development to stereoselectively construct new carbon-carbon bonds across an alkene,[3] which circumvents the use of prefunctionalized organometallic reagents. This strategy enables the expedient synthesis of a range of valuable (hetero)cyclic structures that are frequently found in bioactive compounds.[4–7] Developed methods are mainly restricted to the use of terminal alkenes tethered to an electrophile, in which a chiral ligand enables the enantiodetermining migratory insertion of an organonickel intermediate to foster a single stereogenic center (Scheme 1a). In sharp contrast, the use of internal alkenes presents an inherent challenge for nickel-catalyzed reductive difunctionalization, which could be attributed to several factors.[8] First, the lower reactivity and lower affinity of the internal alkene for nickel often impedes migratory insertion, leading to potential byproducts arising from direct intermolecular reductive cross-coupling between two electrophiles. After an enantioselective migratory insertion step, it could be challenging to achieve a high diastereomeric ratio in the newly formed vicinal stereocenters due to the homolytic character of the alkylnickel intermediate generated in

a) Ni-catalyzed enantioselective difunctionalization of pendant alkenes

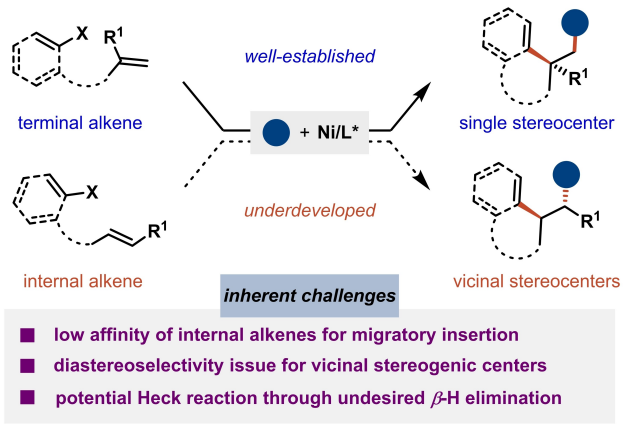

b) This work: Ni-catalyzed enantioselective reductive carbamoyl-alkylation of internal alkenes

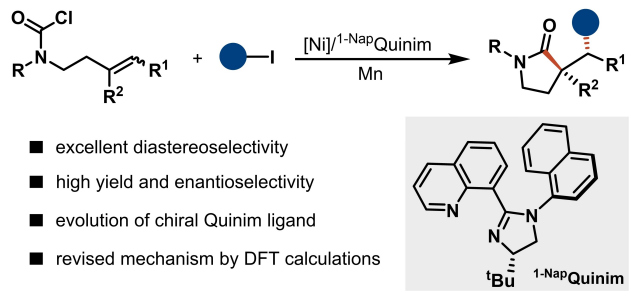

Scheme 1. Ni-catalyzed enantioselective reductive dicarbofunctionalization of alkenes

[*] X. Wu,[+] B. Luan, F. He, J. Qu, Y. Chen
Key Laboratory for Advanced Materials and Joint International Research Laboratory of Precision Chemistry and Molecular Engineering, Feringa Nobel Prize Scientist Joint Research Center, Frontiers Science Center for Materiobiology and Dynamic Chemistry, School of Chemistry and Molecular Engineering, East China University of Science & Technology
Shanghai, 200237 (China)
E-mail: yifengchen@ecust.edu.cn
A. Turlik,[+] K. N. Houk
Department of Chemistry and Biochemistry, University of California
Los Angeles, CA (USA)
E-mail: houk@chem.ucla.edu
[+] These authors contributed equally to this work.

situ.[5j,9] Moreover, the preference for acyclic 1,2-disubstituted alkenes to undergo β-hydride elimination often results in Heck byproducts.[10] Therefore, the enantioselective reductive dicarbofunctionalization of internal alkenes to forge vicinal stereogenic centers would be highly desirable, but has thus far been elusive.[11]

The catalytic enantioselective formation of nitrogen-containing heterocycles remains a long-standing synthetic challenge. Among the various nitrogen heterocycles, the γ-lactam scaffold is one of the most ubiquitous substructures that is found in natural products and pharmaceuticals.[12] The transition metal-catalyzed difunctionalization of alkenes tethered to a carbamoyl electrophile has recently emerged as an appealing strategy for accessing the pyrrolidinone core structure.[13–15] Herein, we report the asymmetric Ni-catalyzed reductive dicarbofunctionalization of internal alkenes with a wide range of primary alkyl iodides to access the pyrrolidinone scaffold bearing vicinal stereogenic centers in good enantiomeric excess and diastereoselectivity under mild conditions (Scheme 1b). Moreover, DFT calculations support a revised reaction mechanism and provide insight into the improvement in enantioselectivity enabled by the modified $^{1\text{-Nap}}$Quinim ligand in the enantiodetermining step for the construction of the pyrrolidinone backbone. These results provide valuable information and a more in-depth understanding of Ni-catalyzed asymmetric reductive cross-coupling reactions.

Results and Discussion

Reaction Optimization

We began our investigations by selecting 1,2-disubstituted alkene-tethered carbamoyl chloride **1a** as the model substrate and primary *n*-heptyl iodide **2a** as the coupling component to optimize the enantioselective synthesis of pyrrolidinone **3a** with vicinal stereogenic centers (Table 1). It was found that the combination of bench-stable $Ni(ClO_4)_2{\bullet}6H_2O$ (15 mol%) and Quinim **L1** (18 mol%) in DMA/MeCN (v/v = 4/1, 0.2 M) with Mn (3.0 equiv) as reductant and LiBr as additive (1.0 equiv) afforded the reductive cyclized cross-coupling product **3a** in 50% corrected GC yield with a promising 90:10 er (entry 1). Importantly, this protocol is highly diastereoselective, with a diastereomeric ratio of >20:1. Intriguingly, introducing an ethyl group at the *ortho* position of the aniline (**L2**) could greatly improve the er to 94.5:5.5. When 1-naphthyl substituted Quinim **L3** was employed, the desired product was obtained in 58% corrected GC yield with 95:5 er, indicating that substitution at the *ortho* position of arenes leads to superior ligands compared to model ligand **L1**. Conversely, commercially available chiral ligands that have been broadly utilized in Ni-catalyzed reductive cross-coupling reactions, such as ^{t}Bu-PHOX **L4** and ^{t}Bu-Biox **L5**, were not effective, while 5-CF_3-^{t}Bu-Pyrox **L6** afforded product **3a** in diminished yield (28%) and much lower enantiomeric excess (38% ee). A mixture of DMA and acetonitrile (DMA/MeCN = 4/1) was more efficient than any single solvent (entries 2–3). Other nickel catalysts such as $Ni(cod)_2$ and $NiBr_2{\bullet}$DME resulted in decreased yield and er (entries 4–5). The identity of the reductant also played a vital role in reaction efficiency, and a poor result was obtained when using Zn instead of Mn (entry 6). The yield of **3a** was improved to 67% and 97:3 er with KI as additive (entry 7). Finally, when the reaction was performed in a DMA/MeCN mixture with Quinim **L3** as supporting ligand, Mn as reductant, and KI as additive under 15 °C, the desired γ-lactam **3a** was obtained in 69% isolated yield (77% GC yield) and 97:3 er (entry 8).

Table 1: Reaction condition optimization.[a]

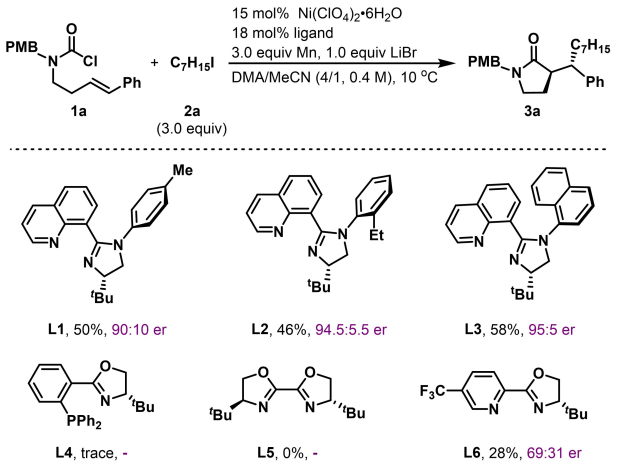

Entry	Deviation from standard condition	**3a** (%)[b]	e.r.[c]
1	none	58	95:5
2	DMA as solvent	51	89:11
3	MeCN as solvent	<5	-
4	$Ni(cod)_2$ instead of $Ni(ClO_4)_2{\bullet}6H_2O$	30	85.5:14.5
5	$NiBr_2{\bullet}$DME instead of $Ni(ClO_4)_2{\bullet}6H_2O$	36	89:11
6	Zn instead of Mn	5	85.5:14.5
7	KI instead of LiBr	67	97:3
8[d]	15 °C	77 (69)	97:3

[a] Reaction conditions: **1a** (0.1 mmol), **2a** (3.0 equiv, 0.3 mmol), [Ni] (15 mol%, 0.015 mmol), ligand (18 mol%, 0.018 mmol), Mn (3.0 equiv, 0.3 mmol), LiBr (1.0 equiv, 0.1 mmol), DMA/MeCN (v/v = 4/1, 0.2 M) under 10 °C for 72 h. [b] The yield was reported as corrected GC yield. [c] The er and dr were determined by HPLC analysis. All the diastereoselectivities are >20:1. [d] $Ni(ClO_4)_2{\bullet}6H_2O$ (20 mol%, 0.020 mmol), **L3** (24 mol%, 0.024 mmol) with 1.0 equiv KI (1.0 equiv, 0.1 mmol) as additive; isolated yield is reported in parentheses.

Substrate Scope

We next used the optimal conditions to explore the substrate scope of the reductive dicarbofunctionalization of 1,2-disubstituted alkenes tethered to carbamoyl chlorides (Scheme 2). Benzyl and alkyl protecting groups on the nitrogen atom were both tolerated, leading to the corresponding products in moderate to good yields with high enantio- and diastereoselectivity (**3a**–**3c**). This protocol was

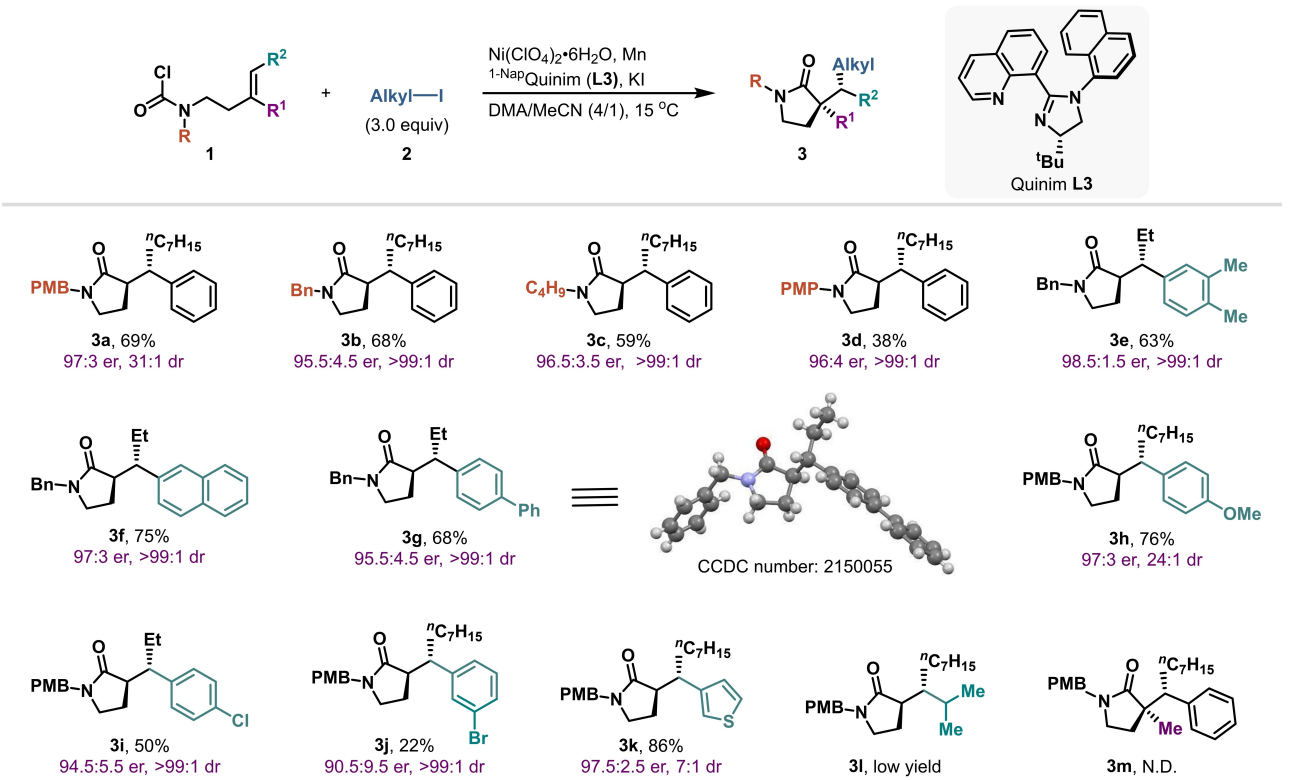

Scheme 2. Substrate scope of Ni-catalyzed enantioselective alkyl-carbamoylation of unactivated 1,2-disubstituted alkenes. Reaction conditions: **1** (1.0 equiv), **2** (3.0 equiv, 0.6 mmol), [Ni] (20 mol%), Quinim **L3** (24 mol%), Mn (3.0 equiv), KI (1.0 equiv), DMA/MeCN (v/v = 4/1, 0.2 M) under 15 °C for the required time.

also suitable for *N-para* methoxy phenyl substituted carbamoyl chloride **3d**. We also investigated the effect of substitution on the aromatic ring tethered to the alkene. Electron-neutral and electron-donating substitutions on the arene did not interfere with consecutive C–C bond formation, providing the corresponding products **3e**–**3h** in good to high yields (63–76%) with excellent enantio- (91–97% ee) and diastereoselectivity (24:1–>99:1). Arenes containing an electron-withdrawing chloride substituent were also able to forge two stereogenic centers (**3i**) in 89% ee and excellent dr (>99:1). However, bromide substitution on the arene caused a sluggish reaction, resulting in a diminished isolated yield (**3j**). Notably, a thiophene-substituted alkene could also be accommodated in this transformation, affording the corresponding product **3k** in 86% yield and 95% ee, albeit with diminished diastereoselectivity (7:1 dr). When an isopropyl-substituted alkene was used under the standard conditions, the desired product **3l** was formed in very low yields (<10%). These data illustrated the necessity of a vinylarene derivative to stabilize the benzylic nickel intermediate. This protocol was not successful with trisubstituted alkene substrate **3m**, presumably because the enantiodetermining migratory insertion step of the carbamoyl-Ni species was hampered by steric hindrance, and thus the reaction proceeded with low conversion; the direct reductive coupling of carbamoyl chloride with alkyl iodide became the main reaction pathway. The X-ray diffraction of **3g**[16] unambiguously confirmed the *R*,*S* configuration of the newly formed stereogenic centers of the pyrrolidinones.

This asymmetric Ni-catalyzed reductive alkyl-carbamoylation of 1,2-disubstituted alkenes was highly diastereoselective. We thus explored the influence of the configuration of aryl alkenes in the starting material on the diastereoselectivity of γ-lactam product **3a** (Scheme 3). Surprisingly, the utilization of both *trans*-alkene **1a** and *cis*-alkene **1n** provided the same pyrrolidinone **3a** with excellent ee and dr (Scheme 3a and 3b). Using the same amount of **1a** and **1n** under the standard conditions also generated the same major diastereoisomer **3a** in 55% yield with 94% ee and 31:1 dr (Scheme 3c). Combined with the above results, we conclude that the stereochemical outcome of the pyrrolidinone product is not correlated to the configuration of the alkene starting material. This can be advantageous for Ni-catalyzed reductive dicarbofunctionalization reactions, since the stereodefined synthesis of internal alkenes is often cumbersome.

The challenging trisubstituted alkene substrate **1m** led us to explore the reactivity of 1,1-disubstituted alkenes. To our delight, the $^{1\text{-Nap}}$Quinim-promoted Ni-catalyzed reductive alkyl-carbamoylation was also suitable for a variety of 1,1-disubstituted alkene-tethered carbamoyl chlorides and primary alkyl iodides under slight modification (Scheme 4). *para*-Methoxy benzyl and secondary cyclohexyl protecting groups on the nitrogen atom of the carbamoyl chlorides were competent in this reaction, affording products **5a** and

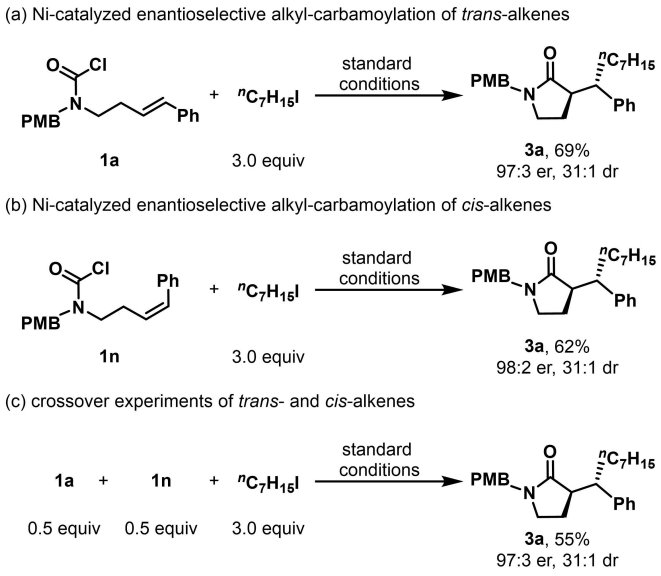

Scheme 3. Influence of configuration of 1,2-disubstituted alkenes towards the outcome of absolute configuration of vicinal disubstituted γ-lactams.

5b with 93% ee. However, using Quinim **L1** provided pyrrolidinone **5a** in diminished 84% ee. The effects of substituents appended to the unactivated alkene moiety were also examined. Alkenes bearing alkyl chains (**5c** and **5d**), benzyl and PMB groups (**5e** and **5f**), and sterically hindered groups including cyclopentyl (**5h**) and cyclohexyl (**5i**) were all suitable substrates for this reaction, affording the corresponding products with high yield and er. Acyclic isopropyl-substituted alkene substrates could also provide **5g** in 63% isolated yield with decreased enantioselectivity (91.5:8.5 er). Sterically hindered isobutyl iodides worked well with high yield and enantioselectivity (**5j**). Functionalized electrophilic coupling partners were then investigated. Alkyl iodides containing a protected ether (**5k**), a cyano group (**5l**), as well as an acetal group (**5m**), were all well-tolerated, furnishing the products with good isolated yield and excellent er. Moreover, a Bpin group (**5n**) that could be employed in further transformations was also compatible with this reductive protocol, which provides more possibilities for the derivatization of the lactam product. Encouragingly, protected amine functionality was also tolerated to afford **5o** in 79% yield with 98.5:1.5 er. It is noteworthy that free N–H groups were tolerated under the reaction conditions: in the case of free N–H containing anilines, the potential side pathway of intermolecular amidation with the reactive carbamoyl chlorides to access urea side products was completely inhibited. It should be noted that tertiary alkyl iodides were not suitable under the standard conditions.

To further demonstrate the synthetic utility of this reductive cross-coupling protocol, the derivatization of α,α-dialkylated pyrrolidinone **5a** was carried out as shown in Scheme 5: thiolactam **6** was obtained in 91% yield through reaction with Lawesson's reagent. X-ray diffraction of **6**[17] unambiguously confirmed the *S* configuration of the thioamide, which indicated the *S* configuration of the

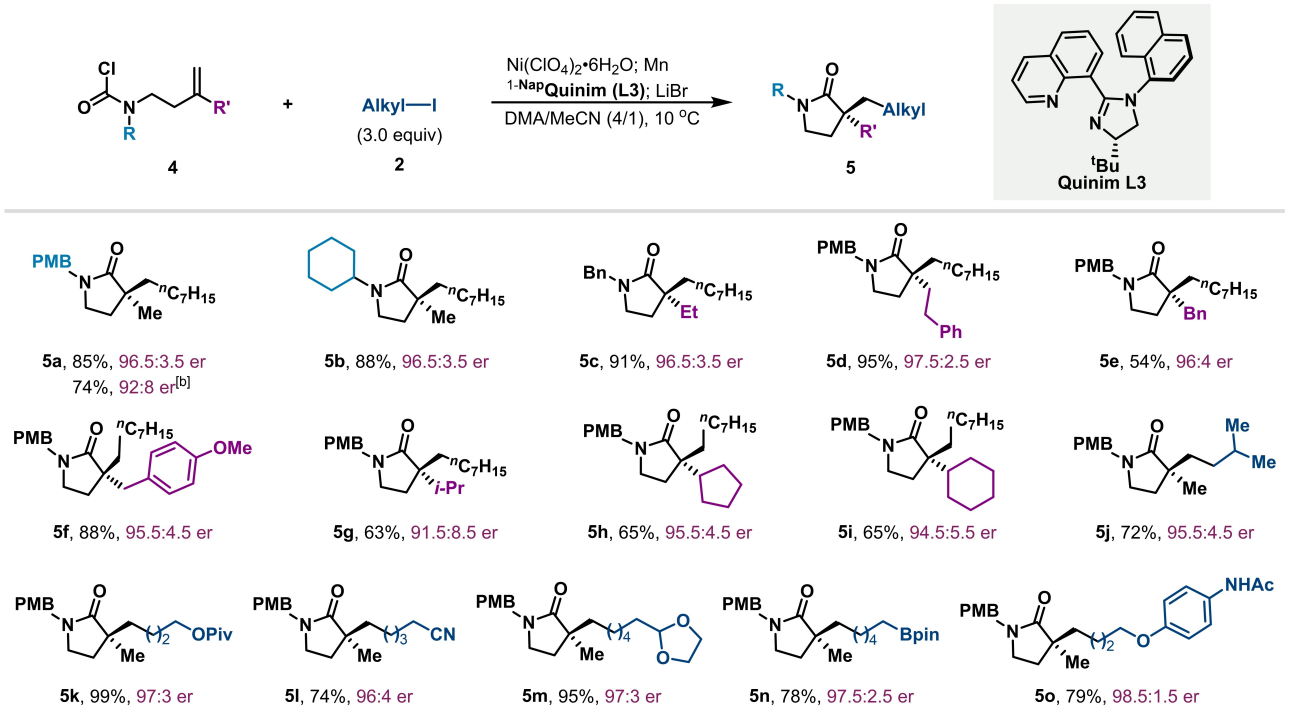

Scheme 4. Substrate scope of Ni-catalyzed enantioselective alkyl-carbamoylation of unactivated alkenes. [a] Reaction conditions: **4** (0.2 mmol), **2** (3.0 equiv, 0.6 mmol), [Ni] (15 mol%, 0.03 mmol), Quinim **L3** (18 mol%, 0.036 mmol), Mn (3.0 equiv, 0.6 mmol), LiBr (1.0 equiv, 0.2 mmol), DMA/MeCN (v/v = 4/1, 0.4 M) under 10 °C for the required time. [b] Quinim **L1** was used instead of Quinim **L3**.

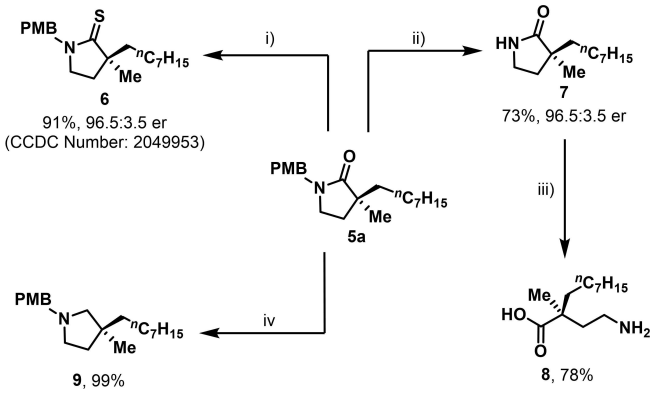

Scheme 5. Derivatization of pyrrolidinone **5a**. Conditions: i) 0.5 equiv Lawesson's reagent, **5a**, toluene, 80 °C, 6 h; ii) 5.0 equiv CAN, **5a**, MeCN/H_2O (5/1), 0 °C, 3 h; iii) a) **7**, 2.0 equiv Boc_2O, 0.5 equiv DMAP, MeCN, rt. b) 10.0 equiv LiOH, THF/H_2O, 50 °C. c) TFA, DCM, rt; iv) 5.0 equiv LAH, THF, 25 °C.

pyrrolidinones. CAN oxidation smoothly cleaved the PMB protecting group of **5a**, affording the unprotected γ-lactam **7** in 73% isolated yield. The ring-opening of lactam **7** provided γ-amino acid **8** bearing a quaternary stereocenter. LAH reduction delivered pyrrolidine **9** in quantitative yield.

Determination of Mechanism by Computational Investigation

Computational Methods

DFT calculations were performed with Gaussian 16.[18] For each structure, conformer searches were performed using CREST[19] in order to identify the lowest-energy conformer. Geometry optimizations were performed with the B3LYP functional[20–24] (which has been shown to perform well in calculations of Ni complexes),[25] augmented with Grimme's D3 empirical dispersion term with Becke-Johnson damping,[26] and the def2-SVP basis set.[27,28] Frequency calculations confirmed the optimized structures as minima (zero imaginary frequencies) or transition state structures (one imaginary frequency) on the potential energy surface. Single point energy corrections were performed using B3LYP-D3(BJ)/def2-TZVPP in the gas phase, which led to close agreement with experimental results. A quasi-harmonic correction was applied using the GoodVibes program.[29]

Enantiodetermining Migratory Insertion

First, we set out to determine the cause of the enantioselectivity observed in the reactions of 1,1-disubstituted alkenes, as shown in Scheme 4. In order to do this, we compared the migratory insertion transition states leading to the two enantiomers (Figure 1a), which we found is the enantiodetermining step in the reaction (the reaction profile is described in more detail in Figure 2).

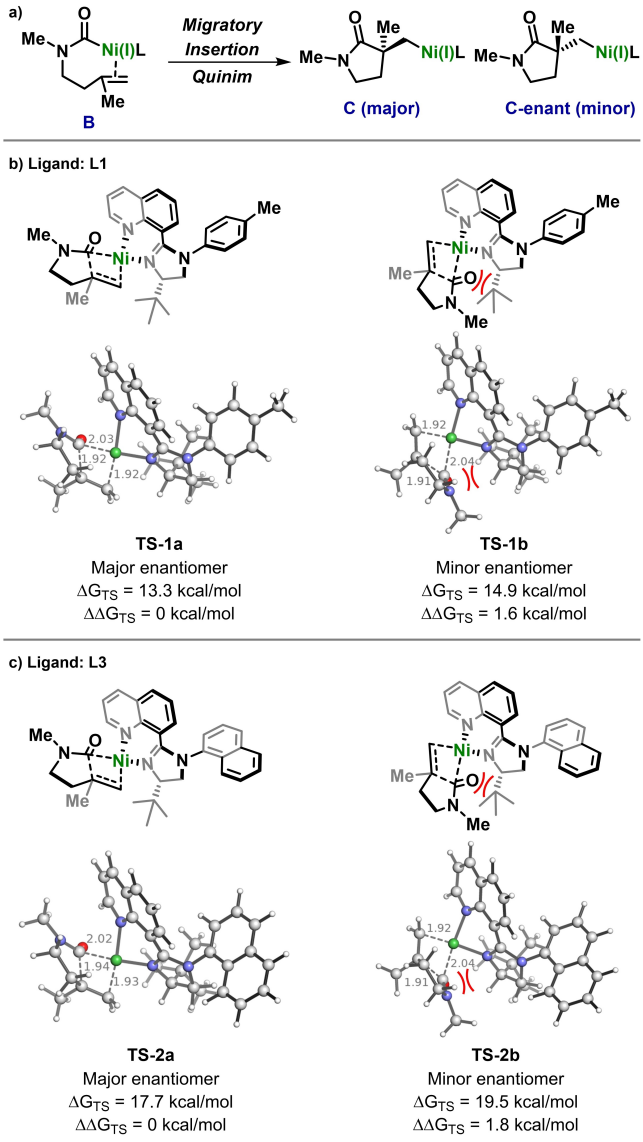

Figure 1. a) Migratory insertion step of model substrate B. b) Comparison of transition states for the formation of two enantiomers with ligand **L1**. c) Comparison of transition states for the formation of two enantiomers with ligand **L3**.

Calculations were first undertaken to determine the factors affecting the enantioselectivity of the reaction using the tolyl ligand, **L1** (Figure 1b). In both the transition state leading to the major enantiomer (**TS-1a**) and that leading to the minor enantiomer (**TS-1b**), the *t*-Bu group on the imidazoline ring fully blocks one side of the ligand system, thus arranging the substrate to occupy the opposite side of the ligand sphere.

The major enantiomer was computed to be favored by 1.6 kcal mol^{-1}, which is consistent with experimental results (92:8 er, which corresponds to a $\Delta\Delta G_{TS}$ of 1.4 kcal mol^{-1}). This preference is hypothesized to arise from strain between the ligand and the substrate in the disfavored transition state, in which unfavorable interactions between the *t*-Bu group of the ligand and the forming lactam ring lead to

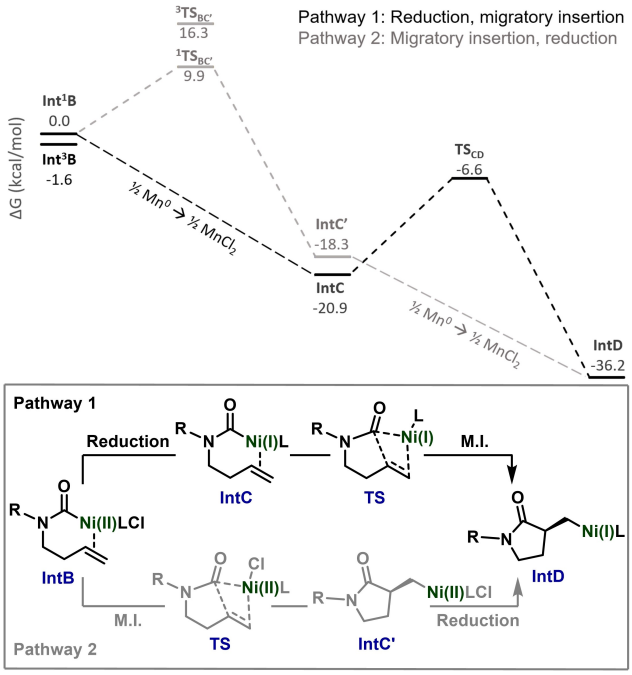

Figure 2. Gibbs free energy profile of two possible pathways for conversion of **IntB** to **IntD**. Energies in kcal mol^{-1}.

distortion of the substrate away from the ligand. In the TS for formation of the minor enantiomer, the carbonyl oxygen is in close proximity to the *t*-Bu group (2.4 Å). Conversely, in the TS leading to the major enantiomer, the substrate is orientated in a manner that positions the carbonyl and the *N*-substituent on the other side of the ligand, near the quinoline fragment. Here, the carbonyl is in close proximity to the aryl-H (2.4 Å away). In addition, the TS leading to the major product favors an orientation in which the alkene is *trans* to the quinoline *N*, whereas in the TS leading to the minor product, the favored TS is one in which the carbonyl C is *trans* to the quinoline *N*.

In order to provide evidence for the hypothesis that a distortion of the substrate occurs in the minor transition state due to unfavorable interactions with the *t*-Bu group, noncovalent interaction regions were plotted using NCI-PLOT (see Supporting Information).[30] Indeed, these plots pointed to significant differences in interactions within two regions between the TS for formation of the major enantiomer and minor enantiomer, where significant interactions occur between the carbonyl of the substrate and the aryl group in the TS for the major enantiomer, and between the *t*-Bu group and the forming lactam ring for the minor enantiomer.

In addition, the effects of removal of the *t*-Bu group were evaluated explicitly. In order to do this, the *t*-Bu group was replaced by a Me group, and a geometry optimization was performed. This caused a significant change in geometry in the TS for the minor enantiomer, particularly between the planes of the ligand N–Ni–N and the substrate C–Ni–C. In the transition state for the reaction with the Me-containing ligand, the forming lactam can relax into a position closer to the ligand sphere. Upon energy calculation with B3LYP-D3(BJ)/def2-TZVPP, the difference in energy between the enantiomers decreased to 0.1 kcal mol^{-1} (compared to 1.6 with the *t*-Bu ligand). This shows that the bulky *t*-Bu group is largely responsible for control of enantioselectivity. In order to test our stereoselectivity model which predicted an 0.1 kcal mol^{-1} difference in transition state barriers between the two enantiomers in the case of the Me-containing ligand, we synthesized this ligand and determined an enantioselectivity of 40:60 er, which would correspond to a $\Delta\Delta G_{TS}$ of −0.2 kcal mol^{-1} and is thus in close agreement with our computational results.

Conversely, when the N–Me group of the substrate was replaced with an N–H in a similar study, there was minimal change in the $\Delta\Delta G_{TS}$ (1.4 kcal mol^{-1}) compared to the original substrate, which indicates that interactions between the N–Me group of the substrate and the imidazoline ring do not contribute significantly to selectivity.

We performed analogous calculations using ligand **L3**—we hypothesized that installing *ortho* substituents on the aryl ring would lead to higher enantioselectivity by forcing the *t*-butyl group towards the forming lactam ring, thus further disfavoring formation of the minor enantiomer. Consistent with experimental results, ligand **L3** was also highly selective, with a $\Delta\Delta G_{TS}$ of 1.8 kcal mol^{-1}, and led to a higher degree of enantioselectivity compared with the original tolyl ligand (**L1**).

Reaction Profile

In addition to analyzing the enantiodetermining step, we studied the reaction profile to determine the mechanism. Here, a model system was used in which the alkene is mono-substituted, and the ligand imidazoline ring is substituted with a phenyl group. The initial oxidative addition of Ni^0 to the C–Cl bond has a transition state barrier of 10.3 kcal mol^{-1}. This reaction is exergonic by 16.8 kcal mol^{-1}. Subsequently, from intermediate **IntB**, two pathways could be envisioned: 1) reduction of Ni^{II} to Ni^{I} by Mn^0 followed by migratory insertion of Ni^{I} to form **IntD**, or 2) migratory insertion of Ni^{II} to form intermediate **IntC'** followed by reduction with Mn^0 (Figure 2). The TS barrier for migratory insertion is low for both pathways: 14.3 kcal mol^{-1} for Pathway 1, and 9.9 kcal mol^{-1} for Pathway 2. Energetically, both of these pathways would be feasible. Calculations of the transition state for the heterogeneous Mn-catalyzed reduction were not possible, but a low transition state barrier for this exergonic transformation is likely. It is noteworthy that the reduction of **IntB** to **IntC** is more exergonic than the reduction of **IntC′** to **IntD**. In order to gain more insight into the mechanism, we studied the migratory insertion transition states for both the $Ni^{II}ClL_n$ and $Ni^{I}L_n$ species. Whereas the migratory insertion of $Ni^{I}L_n$ was consistent with experimental results ($\Delta\Delta G_{TS}$ = 1.5 kcal mol^{-1}), reaction with $Ni^{II}ClL_n$ predicted the opposite enantiomeric outcome ($\Delta\Delta G_{TS}$ = −0.4 kcal mol^{-1}). These data support the mechanism in which reduction of Ni^{II} to Ni^{I} precedes migratory insertion (Pathway 1).

We also studied the energies of triplet states of each Ni^{II} species, as nickel is known to readily access both spin states.[31] In the case of intermediate **IntB**, the triplet state was lower in energy than the singlet by 1.6 kcal mol^{-1}. However, the transition state for migratory insertion with the triplet spin state was significantly higher ($\Delta G =$ 16.3 kcal mol^{-1}), compared to the transition state with the singlet ($\Delta G = 9.9$ kcal mol^{-1}). In order to determine whether the lower-energy triplet state can easily convert to the singlet state, we calculated the minimum energy crossing point between **Int^{3}B** and **Int^{1}B**,[32] and found that the energy required for this transition ($\Delta E = 9.5$ kcal mol^{-1}) was significantly lower than the transition state barrier for migratory insertion with the triplet spin state ($\Delta G_{TS} = 17.9$ kcal mol^{-1}, $\Delta E_{TS} = 18.8$ kcal mol^{-1}). This suggests that if migratory insertion were to occur through Pathway 2, it would proceed through the singlet state. As previously discussed, calculations support a reaction mechanism that proceeds through Pathway 1. Migratory insertion product **IntC′** had a triplet state that was higher in energy than the singlet state by 1.6 kcal mol^{-1}.

Based on the above results, we postulate the following plausible mechanism (Figure 3). First, oxidative addition of the carbamoyl chloride with a low-valent nickel species affords acylnickel(II) species **IntB**, which is then reduced by Mn to provide acyl-Ni^I complex **IntC**. Enantioselective intramolecular migratory insertion followed by a SET process with alkyl iodide affords high-valent alkylnickel(III) species **IntF**. In the case of phenyl-substituted internal alkene substrate **1**, the alkyl-Ni^{III} complex **IntF′** might participate in a fast homolysis of the Ni–C bond to form an alkyl-Ni^{II}/benzylic radical pair that equilibrates rapidly with **IntF**,[5j,9] which might account for the same configuration of pyrrolidinone products resulting from *trans* and *cis* alkenes. The irreversible reductive elimination of **IntF** furnishes the final γ-lactam product with regeneration of the low-valent nickel species.

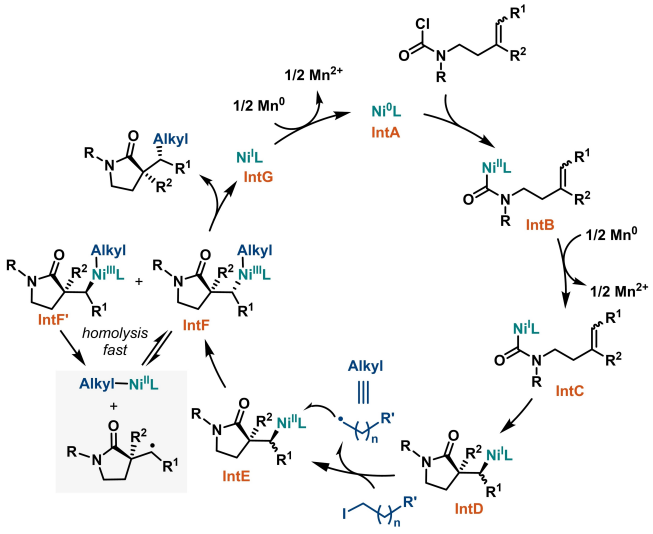

Figure 3. Proposed mechanistic cycle for reductive cyclization.

Conclusion

In summary, we have developed an asymmetric Ni-catalyzed reductive alkyl-carbamoylation reaction of internal alkenes to access various pyrrolidinones bearing vicinal stereocenters in excellent diastereoselectivity. This protocol features broad functional group tolerance under mild reaction conditions. The modification of the Quinim ligand is crucial to obtaining high enantioselectivities. Computational studies support a mechanism in which oxidative addition of Ni to the C–Cl bond is followed by reduction of Ni^{II} to Ni^I, which then undergoes migratory insertion. Migratory insertion is the enantiodetermining step, and the presence of the *t*-butyl group of the ligand leads to distortion of the substrate in the TS leading to the minor enantiomer. Further efforts into Ni-catalyzed intermolecular reductive dicarbofunctionalization of internal alkenes are ongoing in our laboratory.

Acknowledgements

This work was supported by NSFC/China (22171079), the National Science Foundation (grant CHE-1764328), Natural Science Foundation of Shanghai (21ZR1480400), Shanghai Rising-Star Program (20QA1402300), Shanghai Municipal Science and Technology Major Project (Grant No.2018SHZDZX03), the Program of Introducing Talents of Discipline to Universities (B16017) and the China Postdoctoral Science Foundation (2021M701197). A.T. acknowledges the support of the National Institutes of Health under Ruth L. Kirschstein National Research Service Award F32GM134709. Calculations were performed on the Hoffman2 cluster at the University of California, Los Angeles, and the Extreme Science and Engineering Discovery Environment (XSEDE), which is supported by the National Science Foundation (grant OCI-1053575). The authors thank the Analysis and Testing Center of East China University of Science and Technology for help with NMR analysis.

Conflict of Interest

The authors declare no conflict of interest.

Data Availability Statement

The data that support the findings of this study are available in the supplementary material of this article.

Keywords: Density Functional Theory · Internal Alkenes · Lactams · Nickel Catalysis · Vicinal Stereogenic Centers

[1] For selected reviews, see: a) J. R. Coombs, J. P. Morken, *Angew. Chem. Int. Ed.* **2016**, *55*, 2636; *Angew. Chem.* **2016**, *128*, 2682; b) R. K. Dhungana, S. KC, P. Basnet, R. Giri, *Chem. Rec.* **2018**, *18*, 1314.

[2] a) J. Derosa, O. Apolinar, T. Kang, V. T. Tran, K. M. Engle, *Chem. Sci.* **2020**, *11*, 4287; b) X. Qi, T. Diao, *ACS Catal.* **2020**, *10*, 8542; c) Y.-C. Luo, C. Xu, X. Zhang, *Chin. J. Chem.* **2020**, *38*, 1371; d) H.-Y. Tu, S. Zhu, F.-L. Qing, L. Chu, *Synthesis* **2020**, *52*, 1346; e) S. O. Badir, G. A. Molander, *Chem* **2020**, *6*, 1327; f) S. Zhu, X. Zhao, H. Li, L. Chu, *Chem. Soc. Rev.* **2021**, *50*, 10836.

[3] For Ni-catalyzed reductive coupling reviews, see: a) D. A. Everson, D. J. Weix, *J. Org. Chem.* **2014**, *79*, 4793; b) C. E. I. Knappke, S. Grupe, D. Gärtner, M. Corpet, C. Gosmini, A. J. von Wangelin, *Chem. Eur. J.* **2014**, *20*, 6828; c) T. Moragas, A. Correa, R. Martin, *Chem. Eur. J.* **2014**, *20*, 8242; d) D. J. Weix, *Acc. Chem. Res.* **2015**, *48*, 1767; e) J. Gu, X. Wang, W. Xue, H. Gong, *Org. Chem. Front.* **2015**, *2*, 1411; f) J. B. Diccianni, T. Diao, *Trends Chem.* **2019**, *1*, 830; g) K. E. Poremba, S. E. Dibrell, S. E. Reisman, *ACS Catal.* **2020**, *10*, 8237; h) Y. Ping, W. Kong, *Synthesis* **2020**, *52*, 979; i) X. Pang, X. Peng, X.-Z. Shu, *Synthesis* **2020**, *52*, 3751; j) Y. Jin, C. Wang, *Synlett* **2020**, *31*, 1843.

[4] For selected examples of Ni-catalyzed asymmetric reductive cross-coupling, see: a) A. H. Cherney, N. T. Kadunce, S. E. Reisman, *J. Am. Chem. Soc.* **2013**, *135*, 7442; b) A. H. Cherney, S. E. Reisman, *J. Am. Chem. Soc.* **2014**, *136*, 14365; c) Y. Zhao, D. J. Weix, *J. Am. Chem. Soc.* **2015**, *137*, 3237; d) N. T. Kadunce, S. E. Reisman, *J. Am. Chem. Soc.* **2015**, *137*, 10480; e) K. E. Poremba, N. T. Kadunce, N. Suzuki, A. H. Cherney, S. E. Reisman, *J. Am. Chem. Soc.* **2017**, *139*, 5684; f) B. P. Woods, M. Orlandi, C.-Y. Huang, M. S. Sigman, A. G. Doyle, *J. Am. Chem. Soc.* **2017**, *139*, 5688; g) N. Suzuki, J. L. Hofstra, K. E. Poremba, S. E. Reisman, *Org. Lett.* **2017**, *19*, 2150; h) J. L. Hofstra, A. H. Cherney, C. M. Ordner, S. E. Reisman, *J. Am. Chem. Soc.* **2018**, *140*, 139; i) X. Shu, L. Huan, Q. Huang, H. Huo, *J. Am. Chem. Soc.* **2020**, *142*, 19058; j) H. Guan, Q. Zhang, P. J. Walsh, J. Mao, *Angew. Chem. Int. Ed.* **2020**, *59*, 5172; *Angew. Chem.* **2020**, *132*, 5210; k) H. Wang, P. Zheng, X. Wu, Y. Li, T. Xu, *J. Am. Chem. Soc.* **2022**, *144*, 3989.

[5] For recent examples of Ni-catalyzed asymmetric reductive difunctionalization of alkenes, see: a) K. Wang, Z. Ding, Z. Zhou, W. Kong, *J. Am. Chem. Soc.* **2018**, *140*, 12364; b) Y. Jin, C. Wang, *Angew. Chem. Int. Ed.* **2019**, *58*, 6722; *Angew. Chem.* **2019**, *131*, 6794; c) Z.-X. Tian, J.-B. Qiao, G.-L. Xu, X. Pang, L. Qi, W.-Y. Ma, Z.-Z. Zhao, J. Duan, Y.-F. Du, P. Su, X.-Y. Liu, X.-Z. Shu, *J. Am. Chem. Soc.* **2019**, *141*, 7637; d) Y. Ping, K. Wang, Q. Pan, Z. Ding, Z. Zhou, Y. Guo, W. Kong, *ACS Catal.* **2019**, *9*, 7335; e) Y. Li, Z. Ding, A. Lei, W. Kong, *Org. Chem. Front.* **2019**, *6*, 3305; f) T. Ma, Y. Chen, Y. Li, Y. Ping, W. Kong, *ACS Catal.* **2019**, *9*, 9127; g) Y. Jin, H. Yang, C. Wang, *Org. Lett.* **2019**, *21*, 7602; h) J. He, Y. Xue, B. Han, C. Zhang, Y. Wang, S. Zhu, *Angew. Chem. Int. Ed.* **2020**, *59*, 2328; *Angew. Chem.* **2020**, *132*, 2348; i) Y. Jin, H. Yang, C. Wang, *Org. Lett.* **2020**, *22*, 2724; j) D. Anthony, Q. Lin, J. Baudet, T. Diao, *Angew. Chem. Int. Ed.* **2019**, *58*, 3198; *Angew. Chem.* **2019**, *131*, 3230; k) Q. Lin, T. Diao, *J. Am. Chem. Soc.* **2019**, *141*, 17937; l) H.-Y. Tu, F. Wang, L. Huo, Y. Li, S. Zhu, X. Zhao, H. Li, F.-L. Qing, L. Chu, *J. Am. Chem. Soc.* **2020**, *142*, 9604; m) X. Wei, W. Shu, A. García-Domíngues, E. Merino, C. Nevado, *J. Am. Chem. Soc.* **2020**, *142*, 13515; n) L. Guo, M. Yuan, Y. Zhang, F. Wang, S. Zhu, O. Gutierrez, L. Chu, *J. Am. Chem. Soc.* **2020**, *142*, 20390; o) Y. Lan, C. Wang, *Commun. Chem.* **2020**, *3*, 45; p) K. Fang, W. Huang, C. Shan, J. Qu, Y. Chen, *Org. Lett.* **2021**, *23*, 5523; q) T.-Y. Zhao, L.-J. Xiao, Q.-L. Zhou, *Angew. Chem. Int. Ed.* **2022**, *61*, 202115702; *Angew. Chem.* **2022**, *134*, 202115702.

[6] a) X. Wu, J. Qu, Y. Chen, *J. Am. Chem. Soc.* **2020**, *142*, 15654; b) X. Wu, B. Luan, W. Zhao, F. He, X.-Y. Wu, J. Qu, Y. Chen, *Angew. Chem. Int. Ed.* **2022**, *61*, 202111598; *Angew. Chem.* **2022**, *134*, 202111598.

[7] J.-B. Qiao, Y.-Q. Zhang, Q.-Y. Yao, Z.-Z. Zhao, X. Peng, X.-Z. Shu, *J. Am. Chem. Soc.* **2021**, *143*, 12961.

[8] For selected racemic examples of Ni-catalyzed dicarbofuntionalization of internal alkenes, see: a) J. Derosa, V. T. Tran, M. N. Boulous, J. S. Chen, K. M. Engle, *J. Am. Chem. Soc.* **2017**, *139*, 10657; b) R. K. Dhungana, R. R. Sapkota, L. M. Wickham, D. Niroula, R. Giri, *J. Am. Chem. Soc.* **2020**, *142*, 20930; c) R. K. Dhungana, R. R. Sapkota, L. M. Wickham, D. Niroula, B. Shrestha, R. Giri, *Angew. Chem. Int. Ed.* **2021**, *60*, 22977; *Angew. Chem.* **2021**, *133*, 23159; d) Z.-Q. Li, W.-J. He, H.-Q. Ni, K. M. Engle, *Chem. Sci.* **2022**, *13*, 6567; e) Z.-Q. Li, Y. Cao, T. Kang, K. M. Engle, *J. Am. Chem. Soc.* **2022**, *144*, 7189; f) T. Kang, J. M. González, Z.-Q. Li, K. Foo, P. T. W. Cheng, K. M. Engle, *ACS Catal.* **2022**, *12*, 3890.

[9] a) O. Gutierrez, J. C. Tellis, D. N. Primer, G. A. Molander, M. C. Kozlowski, *J. Am. Chem. Soc.* **2015**, *137*, 4896; b) Y. He, C. Liu, L. Yu, S. Zhu, *Angew. Chem. Int. Ed.* **2020**, *59*, 21530; *Angew. Chem.* **2020**, *132*, 21714.

[10] a) S. Bhakta, T. Ghosh, *Adv. Synth. Catal.* **2020**, *362*, 5257; b) M. R. Kwiatkowski, E. J. Alexanian, *Angew. Chem. Int. Ed.* **2018**, *57*, 16857; *Angew. Chem.* **2018**, *130*, 17099; c) J. M. Medina, J. Moreno, S. Racine, S. Du, N. K. Garg, *Angew. Chem. Int. Ed.* **2017**, *56*, 6567; *Angew. Chem.* **2017**, *129*, 6667; d) J.-N. Desrosiers, L. Hie, S. Biswas, O. V. Zatolochnaya, S. Rodriguez, H. Lee, N. Grinberg, N. Haddad, N. K. Yee, N. K. Garg, C. H. Senanayake, *Angew. Chem. Int. Ed.* **2016**, *55*, 11921; *Angew. Chem.* **2016**, *128*, 12100.

[11] a) X. Mu, Y. Shibata, Y. Makida, G. C. Fu, *Angew. Chem. Int. Ed.* **2017**, *56*, 5821; *Angew. Chem.* **2017**, *129*, 5915; b) H. Huo, B. J. Gorsline, G. C. Fu, *Science* **2020**, *367*, 559; c) L. An, F.-F. Tong, S. Zhang, X. Zhang, *J. Am. Chem. Soc.* **2020**, *142*, 11884.

[12] For selected reviews, see: a) L.-W. Ye, C. Shu, F. Gagosz, *Org. Biomol. Chem.* **2014**, *12*, 1833; b) J. Caruano, G. G. Muccioli, R. Robiette, *Org. Biomol. Chem.* **2016**, *14*, 10134; c) G. Pandey, A. Mishra, J. Khamrai, *Tetrahedron* **2018**, *74*, 4903.

[13] a) M. Shrestha, X. Wu, W. Huang, J. Qu, Y. Chen, *Org. Chem. Front.* **2021**, *8*, 4024; b) S. M. Hande, M. Nakajima, H. Kamisaki, C. Tsukano, Y. Takemoto, *Org. Lett.* **2011**, *13*, 1828; c) C. Chen, J. Hu, J. Su, X. Tong, *Tetrahedron Lett.* **2014**, *55*, 3229; d) X. Wu, Z. Tang, C. Zhang, C. Wang, L. Wu, J. Qu, Y. Chen, *Org. Lett.* **2020**, *22*, 3915; e) C. Zhang, X. Wu, C. Wang, C. Zhang, J. Qu, Y. Chen, *Org. Lett.* **2020**, *22*, 6376; f) C. Wang, W. Zhao, X. Wu, J. Qu, Y. Chen, *Adv. Synth. Catal.* **2020**, *362*, 4996; g) J. F. Rodríguez, A. Zhang, J. Bajohr, A. Whyte, B. Mirabi, M. Lautens, *Angew. Chem. Int. Ed.* **2021**, *60*, 18478; *Angew. Chem.* **2021**, *133*, 18626.

[14] a) P. Fan, Y. Lan, C. Zhang, C. Wang, *J. Am. Chem. Soc.* **2020**, *142*, 2180; b) A. Whyte, K. I. Burton, J. Zhang, M. Lautens, *Angew. Chem. Int. Ed.* **2018**, *57*, 13927; *Angew. Chem.* **2018**, *130*, 14123; c) A. D. Marchese, M. Wollenburg, B. Mirabi, X. Abel-Snape, A. Whyte, F. Glorius, M. Lautens, *ACS Catal.* **2020**, *10*, 4780; d) J. Wu, C. Wang, *Org. Lett.* **2021**, *23*, 6407; e) Z. Feng, Q. Li, L. Chen, H. Yao, A. Lin, *Sci. China Chem.* **2021**, *64*, 1367.

[15] Y. Li, F.-P. Zhang, R.-H. Wang, S.-L. Qi, Y.-X. Luan, M. Ye, *J. Am. Chem. Soc.* **2020**, *142*, 19844.

[16] The crystal structure has been deposited with The Cambridge Crystallographic Data Centre (Deposition Number 2150055).

[17] The crystal structure has been deposited with The Cambridge Crystallographic Data Centre (Deposition Number 2049953).

[18] M. J. Frisch, G. W. Trucks, H. B. Schlegel, G. E. Scuseria, M. A. Robb, J. R. Cheeseman, et al. Wallingford, CT; **2016**.

[19] P. Pracht, F. Bohle, S. Grimme, *Phys. Chem. Chem. Phys.* **2020**, *22*, 7169.

[20] S. H. Vosko, L. Wilk, M. Nusair, *Can. J. Phys.* **1980**, *58*, 1200.

[21] M. Head-Gordon, J. A. Pople, M. J. Frisch, *Chem. Phys. Lett.* **1988**, *153*, 503.

[22] C. Lee, W. Yang, R. G. Parr, *Phys. Rev. B* **1988**, *37*, 785.
[23] A. D. Becke, *J. Chem. Phys.* **1993**, *98*, 5648.
[24] P. J. Stephens, F. J. Devlin, C. F. Chabalowski, M. J. Frisch, *J. Phys. Chem.* **1994**, *98*, 11623.
[25] M. Steinmetz, S. Grimme, *ChemistryOpen* **2013**, *2*, 115.
[26] S. Grimme, S. Ehrlich, L. Goerigk, *J. Comput. Chem.* **2011**, *32*, 1456.
[27] F. Weigend, R. Ahlrichs, *Phys. Chem. Chem. Phys.* **2005**, *7*, 3297.
[28] F. Weigend, *Phys. Chem. Chem. Phys.* **2006**, *8*, 1057.
[29] G. Luchini, J. Alegre-Requena, I. Funes, J. Rodríguez-Guerra, J. Chen, R. Paton, *Zenodo* **2019**; https://doi.org/10.5281/zenodo.3346166.
[30] J. Contreras-García, E. R. Johnson, S. Keinan, R. Chaudret, J.-P. Piquemal, D. N. Beratan, W. Yang, *J. Chem. Theory Comput.* **2011**, *7*, 625.
[31] For an example of the importance of singlet-triplet spin-switching in Ni-catalyzed reactions, see: A. K. Vitek, A. K. Leone, A. J. McNeil, P. M. Zimmerman, *ACS Catal.* **2018**, *8*, 3655.
[32] a) J. N. Harvey, M. Aschi, H. Schwarz, W. Koch, *Theor. Chem. Acc.* **1998**, *99*, 95; b) J. Rodríguez-Guerra, *Zenodo* **2020**. https://doi.org/10.5281/zenodo.4293422.

Manuscript received: May 22, 2022
Accepted manuscript online: July 11, 2022
Version of record online: July 25, 2022